

Ab initio simulations of hydrogenated amorphous silicon

Karol Jarolimek^{*‡}, Robert A. de Groot[†], Gilles A. de Wijs[†] and Miro Zeman[‡]

^{*} Electronic Structure of Materials, IMM,
Radboud University Nijmegen,
Toernooiveld 1, 6525 ED Nijmegen,
The Netherlands

Email: k.jarolimek@science.ru.nl

[†] Electronic Structure of Materials, IMM,
Radboud University Nijmegen,
Toernooiveld 1, 6525 ED Nijmegen,
The Netherlands

[‡] Delft University of Technology, DIMES,
Feldmannweg 17, 2600 GB Delft,
The Netherlands

Abstract—Our research is aimed at investigating multilayers of hydrogenated amorphous silicon (a-Si:H) and hydrogenated amorphous silicon nitride (a-Si_xN_y:H). We are particularly interested in the interface between these two materials and in calculating the band offset. Multilayered structures can be used as selective energy contacts and/or selective absorbers of light in the new generation of thin film solar cells. The multilayers can be tuned to absorb visible light of certain wavelength by modifying the concentration of nitrogen in a-Si_xN_y:H and/or thickness of a-Si_xN_y:H layers. To be able to model the a-Si:H/a-Si_xN_y:H interface we first need to obtain a realistic amorphous structure of a-Si:H. Our approach to simulate the electronic structure of a-Si:H is based on a molecular dynamics (MD) simulation within the Density Functional Theory (DFT) approximation. This method is referred to as *ab initio* i.e. it requires no input from experiment. The procedure consists of heating the crystalline silicon structure to 2370 K, creating a liquid and then cooling it down to room temperature. The effect of the cooling rate is examined. We were able to prepare a realistic amorphous structure which compares well to experimental data obtained by neutron scattering experiments. For the first time a band gap is observed in a-Si:H with hydrogen atomic concentration of 11%.

I. INTRODUCTION

Hydrogenated amorphous silicon (a-Si:H) has a number of promising properties. The absorption coefficient is higher by almost two orders of magnitude in the visible part of the spectrum than in crystalline silicon [1]. This property is being exploited in production of solar cells. The higher absorption coefficient means less material in order to absorb the same amount of light thus allowing for use of films less than 1 micrometer thick. Another advantage of a-Si:H films is that they are deposited at low substrate temperatures using large-area plasma enhanced chemical vapor deposition technology. This not only reduces the price of the cells but also it makes possible to fabricate them on flexible substrates. Another tempting property of all amorphous alloys is the growth of multilayers of arbitrary composition, since there is no need

for lattice alignment. This enables the preparation of new materials with desired optical properties.

These considerations motivate this work for a fundamental understanding of intrinsic properties of a-Si:H. The theoretical approaches in modeling of amorphous materials are based mostly on cooling of liquid samples. The accuracy of such simulations ranges from simple classical molecular dynamics using model potentials to state of the art *ab initio* molecular dynamics. Wooten, Winer and Weaire proposed a novel bond switching algorithm (WWW algorithm) [2], which does not fit in any of the previous categories. In the following we will briefly discuss these approaches.

II. CLASSICAL MOLECULAR DYNAMICS

Within classical molecular dynamics (MD) the interaction between the atoms is expressed through empirical potentials. Atoms and molecules are treated purely in terms of classical mechanics. The forces and total energy are obtained from the potentials and inserted into Newton's law which is solved numerically to calculate the evolution of atomic coordinates in time. Several types of potentials are used, including the three body potentials of Keating [3] and Stillinger–Weber [4]. The most commonly used potential is the Tersoff [5] potential which goes beyond the two and three body potentials and is able of predicting wider variety of structures (e.g. liquid silicon). The flexibility of this type of potential arises from the fact that its form depends on the effective coordination, or in other words on the local environment in which the atom is placed. It was later improved by Ohira et al. [6] to include also silicon–hydrogen and hydrogen–hydrogen interactions. Recently a Tersoff type potential was used to study silicon oxides and oxinitrides [7]. The parameters of the empirical potential were fitted using Density Functional Theory (DFT) calculations on a set of diverse systems and configurations (e.g. SiH₃, Si₃N₄). The main advantage of classical MD is

that longer simulation schemes for investigated systems are feasible. It is even possible to model the thin film growth by impingement of SiH_3 radicals onto silicon surface [8]. The upper limit of the simulation time is ~ 1 ns which seems to be sufficient for the silicon atoms to relax fully to form a realistic amorphous structure. This also implies the possibility to perform the heating and cooling in a less abrupt way. The weakest point of classical MD stays the potential which is used. Clearly it is impossible to create a potential that would mimic all the diverse structures and chemical reactions that occur during the film growth. Some groups implement a combination of classical and *ab initio* MD [9]. They start with a classical MD, benefit from the long heating / cooling scheme and than use *ab initio* methods to relax the structure to the nearest local minimum.

III. *Ab initio* MD

In *ab initio* MD forces and energies are obtained by solving the Schrödinger equation for the quantum mechanical ground state of the system. Unlike classical MD fitting of the potential to empirical data is not needed. In principle the only input for the calculation are the initial positions and velocities of atoms and their masses. Amorphous silicon is usually prepared by simulated quenching from liquid silicon. Since the pioneering work of Car and Parrinello [10] there have been more studies which followed this procedure [11], [12], [13], [14], [15], [16], [17]. The *ab initio* MD being more accurate and much more expensive is limited to simulation times of the order of 10 ps and typically with no more than a hundred of atoms. This corresponds to cooling rates of ~ 1 K/fs which is about 100 times faster than rates used to prepare a-Si by laser glazing techniques. The result is an increased number of coordination defects in the supercell. To overcome this problem Valladares et al. [18] proposed a novel heating/cooling scheme, called the undermelt quench method. The main idea is to heat the silicon material just to the temperature of 1685 K which is well above the glass transition temperature but under the melting point of c-Si. Silicon has the favorable property that the melting temperature of a-Si is 250 K lower than the melting temperature of c-Si. Another fact that supports this approach is that liquid silicon has much different properties than the amorphous silicon (e.g it has a metallic character, coordination number between 6 and 7). However, using this procedure one has to exhibit care to fully melt the periodic lattice. Otherwise one could partially restore the crystalline structure after the cooling.

IV. WWW ALGORITHM

The bottleneck of MD approaches is that they typically end up with a structure with an unrealistic concentration of coordination defects. The concentration of defects typically found in device quality material is $\sim 10^{17} \text{cm}^{-3}$ which corresponds to 1 defect per $\sim 10^6$ atoms. From this follows that simulation supercells with ~ 100 atoms have to be defect free. The WWW algorithm as proposed in the original paper of Wooten, Winer and Weaire [2] tries to overcome the problem

TABLE I
POSITION OF ATOMS IN C-SI:H CELL. THE COORDINATES ARE IN REDUCED UNITS.

atom	x	y	z
Si	0.00	0.00	0.00
Si	0.00	0.50	0.50
Si	0.50	0.00	0.50
Si	0.50	0.50	0.00
Si	0.25	0.25	0.25
Si	0.75	0.25	0.75
Si	0.25	0.75	0.75
Si	0.75	0.75	0.25
H	0.50	0.50	0.50

of unrealistic defect concentrations by the creation of so called continuum random networks. These networks are structures with preserved four fold bonding (i.e. every silicon atom has four bonds, there exist no dangling or floating bonds). The WWW algorithm is very successful in creating high quality amorphous structures in good agreement with experiment at low computational cost. The model was further improved by Barkema and Mousseau [19], who succeeded in preparation of a 4096 atom high quality structure. This approach is applied mostly on one compound materials and to our knowledge no study on hydrogenated amorphous silicon has been performed.

V. PREPARATION OF THE STRUCTURE

Hydrogen plays a vital role in saturating dangling bonds and removing electronic spectral defect states inside the gap. A typical device quality material has a hydrogen concentration of 11%. In this case the use of the WWW approach would be awkward, since there are no dangling bonds to saturate (all silicon atoms have four neighbors). Bearing in mind that our long term goal is to model interfaces of amorphous silicon and amorphous silicon nitride we choose the *ab initio* MD because of its accuracy and universality. The diverse local environments present in the interface would impose too high demands on a classical model potential.

We start our preparation procedure with a periodically repeated cubic supercell containing 64 silicon and 8 hydrogen atoms. The supercell is build of eight c-Si:H cells each comprising eight silicon and one hydrogen atom. The c-Si:H cell is in fact a cubic unit cell of crystalline silicon with one hydrogen atom in the middle (see Table I). The side of the supercell is set to 11.062 \AA to reproduce the experimental density value of 2.20 g/cm^3 . The total energy and forces are calculated within the DFT Generalized Gradient Approximation (GGA). We used the Vienna *Ab initio* Simulation Program (VASP) [20], [21]. Electron-ion interactions were described using the projector augmented wave method [22], [23]. The energy cutoff was set to 200 eV. During the whole MD run we use only the Γ point for Brillouin zone sampling.

Essentially the mode with the highest vibrational frequency which can occur during the simulation is the vibration of the hydrogen molecule. The second highest frequency of vibration occurs when a hydrogen atom is attached to a 3 bonded silicon atom. We set our time step to 1 fs which proves

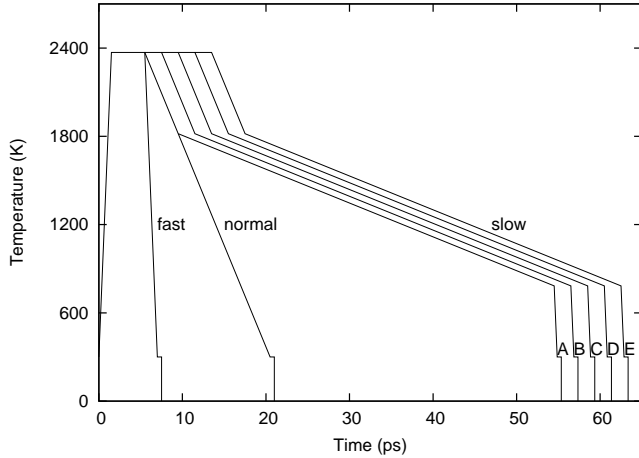


Fig. 1. The heating / cooling scheme used to prepare three samples with fast, normal and slow cooling rate. The five slow quench samples are marked with letters A, B, C, D and E.

to be sufficient to describe the latter case. The integration of vibrational motion of the hydrogen molecule using this time step is rather crude. However the time step of 1 fs is a reasonable compromise between computational cost and accuracy.

The heating and cooling of the structure was done by velocity rescaling on every MD step. The thermal procedure begins at 300 K. The velocities are initialized randomly according to a Maxwell–Boltzmann distribution. The structure is then heated to 2370 K in 1.5 ps which corresponds to a heating rate of 1.380 K/fs. At this temperature the system is a liquid. We find that the liquid sample is a metal with no trace of a gap in the density of states. This is consistent with previous calculations [11]. In order to destroy any trace of crystallinity we let the system evolve for 4 ps. In the next step the system is cooled back to 300 K. We study that for three different cases. In the first case the rate is identical to the heating rate (1.380 K/fs). In the second case we cool the structure to 300 K in 15 ps resulting in a ten times slower rate (0.138 K/fs). In the last cooling procedure we are actually using three different rates. From 2370 K to 1818 K we follow the 0.138 K/fs rate, from 1818 K to 783 K we apply the 0.023 K/fs rate and finally from 783 K to 300K we apply the rate 1.380 K/fs (see Fig. 1). The use of three different rates is motivated by preparing a high quality amorphous structure in a shortest time. In the first temperature interval the silicon atoms still exhibit a strong liquid like behavior. In the second interval, being the most important, the rate used is as small as possible to allow even improbable relaxation events to occur. In the last temperature interval the atoms exhibit only vibrational movement with no chance of a further relaxation. Consequently we use the fastest cooling rate to save computer time. After reaching the room temperature the system is evolved for 0.5 ps to calculate structural averages e.g. pair correlation function, bond angle distribution function and static structure factor. The bond angle distribution function gives

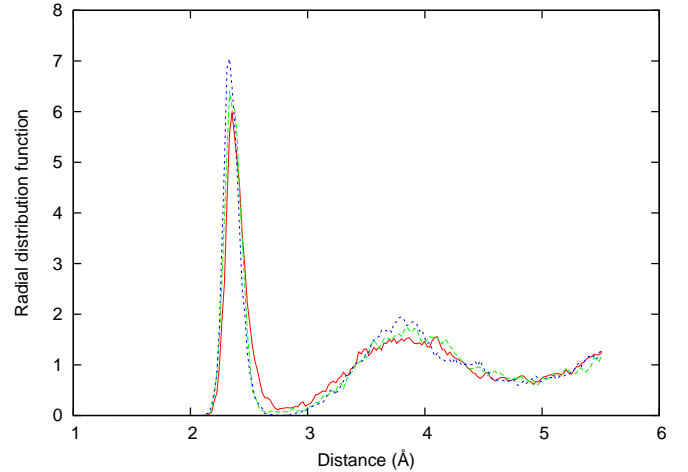


Fig. 2. Partial radial distribution function Si-Si of three structures prepared by fast (solid red line), normal (dashed green line) and slow cooling rate (dotted blue line).

a distribution of angles between two silicon–silicon bonds connected to a common silicon atom. The static structure factor is a quantity proportional to the diffracted intensity in an x-ray or neutron diffraction experiment. After calculating the structural averages the amorphous structure is relaxed using the conjugated gradient method and electronic properties are calculated.

VI. EFFECT OF THE COOLING RATE

To examine the effect of the cooling rate on the quality of the amorphous structure we employ three distinct rates: 1.380 K/fs, 0.138 K/fs and 0.023 K/fs. We will refer to these rates as the fast, normal and slow cooling rate.

A useful measure of short range order in amorphous structures is the radial distribution function $g(r)$. It gives the probability of finding two atoms at a distance r apart. For a binary system like a-Si:H there are three partial radial distribution functions i.e. $g_{Si-Si}(r)$, $g_{Si-H}(r)$ and $g_{H-H}(r)$. We show the silicon–silicon radial distribution function for different cooling rates in Fig. 2. We observe that the slower cooling results in better defined peaks with higher values of the first and second maximum of $g_{Si-Si}(r)$. With slower cooling rates the value of the first minimum in $g_{Si-Si}(r)$ is decreasing towards zero. To proceed any further we need to define a cutoff distance for silicon–silicon and silicon–hydrogen bond. If a distance between two atoms is smaller than the cutoff distance they are considered to be bonded. The cutoff distance of the silicon–silicon bond was set to 2.76 Å corresponding to the position of the first minimum in $g_{Si-Si}(r)$. Similarly the cutoff distance of the silicon–hydrogen bond was set to 1.79 Å matching the position of the first minimum in $g_{Si-H}(r)$. The cooling rate does not change the position of the first minimum in $g_{Si-Si}(r)$ and $g_{Si-H}(r)$ functions what facilitates the use of same cutoff distances for all the prepared samples. The calculated values of the coordination number N_c , the mean nearest–neighbor distance \bar{r} and the root–mean square (RMS) bond length deviation σ_r show an improvement with experiment for the

TABLE II

STRUCTURAL PROPERTIES OF SAMPLES PREPARED BY FAST, NORMAL AND SLOW COOLING RATES: COORDINATION NUMBER N_c , MEAN NEAREST-NEIGHBOR DISTANCE \bar{r} , RMS BOND LENGTH DEVIATION σ_r , MEAN BOND ANGLE $\bar{\theta}$ AND RMS BOND ANGLE DEVIATION σ_θ COMPARED TO EXTENDED X-RAY ABSORPTION FINE STRUCTURE (EXAFS) EXPERIMENT.

structure	N_c	\bar{r}	σ_r	$\bar{\theta}$	σ_θ
fast	3.94	2.40	0.10	107.40	19.07
normal	3.83	2.37	0.08	108.57	14.59
slow	3.87	2.36	0.08	108.63	14.25
exp. Ref. [24]	3.88	2.35	0.07	–	–

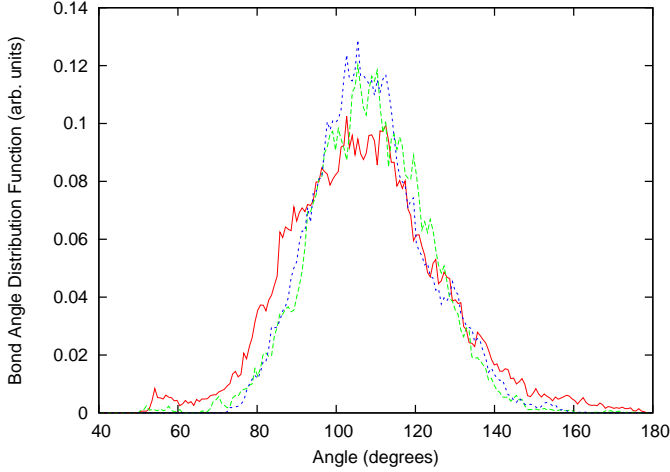


Fig. 3. Bond angle distribution function of three structures prepared by fast (solid red line), normal (dashed green line) and slow (dotted blue line) cooling rates.

normal and slow cooling rate. (see Table II). The coordination number is defined as

$$N_c = \int_0^{r_m} 4\pi\rho r^2 g_{Si-Si}(r) dr,$$

where ρ is the atomic density and r_m is the cutoff distance of the silicon–silicon bond. Further, we calculate the bond angle distribution function (see Fig. 3). The peak centered around the tetrahedral bond angle narrows with slower cooling rate. The RMS bond angle deviation is changing from 19.07° to 14.25° for fast and slow cooling rates respectively. Note that the sample prepared by fast cooling rate has also a peak at 55° . This is a residue of the metallic bonding in the liquid. The healing power of slow cooling is even more visible in the electronic properties. The number of structural defects responsible for the ingap states decreases with slower cooling (see Table III). This trend can be also followed in the calculated density of states (see Fig. 4). We used a $5\times 5\times 5$ Monkhorst–Pack mesh for the Brillouin Zone sampling and Gaussian broadening of 0.05 eV. Note that the slow quench structure has neither structural defects nor spectral defect states in the gap. The tendency of improving the quality of the structure with slower cooling is exactly what one would expect. However what is not so obvious is whether the rate of the order of 0.01 K/fs is sufficient. Based on the properties of the slow quench structure presented above we think it is.

TABLE III

TYPES OF NEIGHBORING ENVIRONMENTS FOR THREE STRUCTURES PREPARED BY FAST, NORMAL AND SLOW COOLING RATES. THE EXPRESSION Si_3H_1 DENOTES THAT THE GIVEN ATOM HAS A TOTAL NUMBER OF FOUR NEIGHBORS, THREE OF WHICH ARE SILICON ATOMS AND ONE IS A HYDROGEN ATOM.

structure	Si_2H_2	Si_3H_0	Si_3H_1	Si_4H_0	Si_4H_1	Si_5H_0
fast	1	0	6	55	0	2
normal	0	3	7	53	1	0
slow	1	0	4	59	0	0

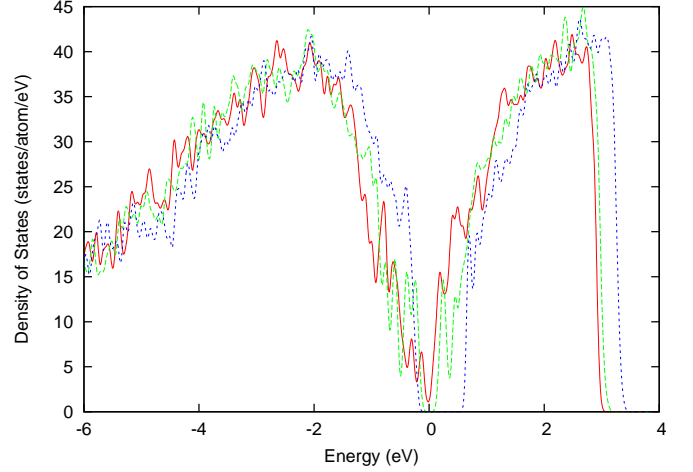


Fig. 4. Density of states of three structures prepared by fast (solid red line), normal (dashed green line) and slow (dotted blue line) cooling rates. The Fermi energy is set to 0 eV.

VII. STRUCTURES OBTAINED BY SLOW QUENCHING

We prepared a total of five structures using the slow cooling rate. We will denote these structures as A, B, C, D and E (see Fig. 1). They all start from different liquid configurations separated in time by 2 ps at the temperature 2370 K. The radial distribution functions as well as the static structure factors are averaged over the five slowly quenched samples and compared with neutron diffraction measurements [25]. We calculate the three partial static structure factors according to the definition of Ashcroft and Langreth:

$$S_{ij}(q) = \frac{1}{\sqrt{N_i}} \frac{1}{\sqrt{N_j}} \left[\left\langle \sum_{\mu}^{N_i} \sum_{\nu}^{N_j} e^{-i\vec{q}\cdot(\vec{R}_{i\mu} - \vec{R}_{j\nu})} \right\rangle - \delta_{\vec{q},\vec{0}} \right],$$

where N_i and N_j denote number of atoms of species i and j respectively, \vec{R} are the position vectors of atoms and \vec{q} is a vector in reciprocal space. The averaging is performed over different \vec{q} which have the same length. As seen in Fig. 5 the agreement between theoretical and experimental silicon–silicon structure factor is excellent. We are able to reproduce the first two peaks as well as the following peaks up to 15 \AA^{-1} . The agreement is worse for the remaining partial static structure factors. This is due to the use of a very small number of hydrogen atoms, resulting in a poor statistics. By performing a Fourier transform of the static structure factor one obtains the radial distribution function. The fact that the experimental static structure factors are

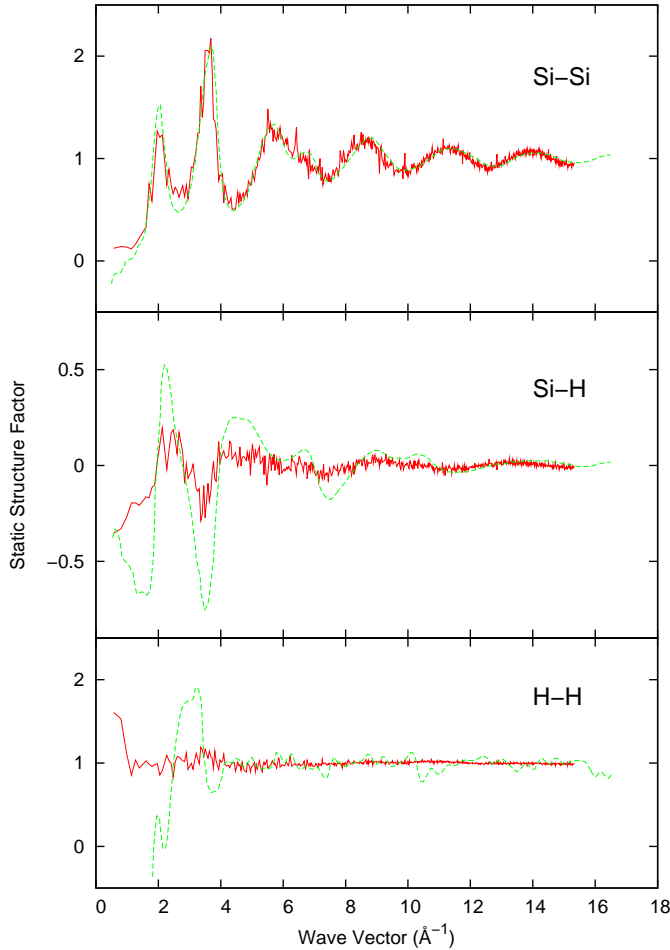


Fig. 5. Partial static structure factors averaged over five slow quench samples (red solid line) and compared to neutron scattering measurements [25] (green dashed line). Both curves refer to systems at 300 K.

measured over a finite interval in reciprocal space, results in unphysical negative values of the radial distribution function at small distances. We find an excellent agreement between the calculated and measured silicon–silicon radial distribution function (see Fig. 6). The positions of the first and second maximum in $g_{Si-Si}(r)$ are 2.34 Å and 3.82 Å respectively and coincide with the measured values. The calculated position of the first peak in the silicon–hydrogen radial distribution function is found to be 1.51 Å. We note that the calculated value 1.51 Å is identical to the silicon–hydrogen bond length in the silane molecule. The calculated hydrogen–hydrogen radial distribution function has a peak at 0.75 Å corresponding to the hydrogen molecule bond. Hydrogen molecules are found in samples A and D. Again the statistics in the hydrogen–hydrogen radial distribution function is very poor rendering any comparisons with the experiment unreliable. In Table IV we summarize structural properties of the slow quench samples and compare them to EXAFS measurements.

Two of the five prepared samples, namely A and C, have no structural defects (see Table V). The remaining samples have

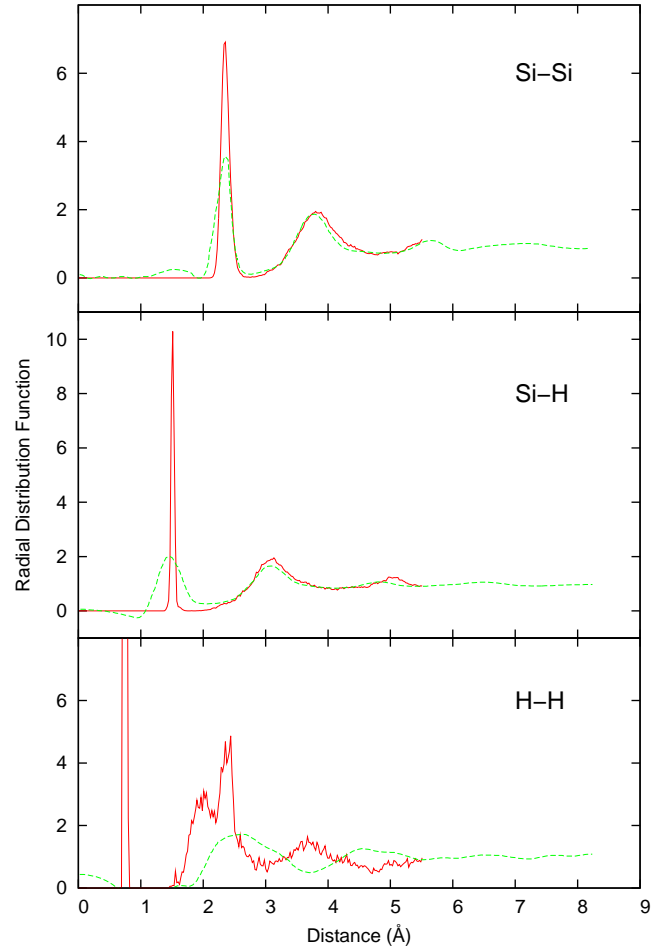


Fig. 6. Partial radial distribution functions averaged over five slow quench samples (red solid line) and compared to neutron scattering measurements [25] (green dashed line). Both curves refer to systems at 300 K.

TABLE IV
STRUCTURAL PROPERTIES OF THE FIVE SAMPLES PREPARED BY SLOW COOLING RATE: COORDINATION NUMBER N_c , MEAN NEAREST-NEIGHBOR DISTANCE \bar{r} , ROOT MEAN SQUARE DEVIATION OF THE BOND LENGTH σ_r , MEAN BOND ANGLE $\bar{\theta}$ AND ROOT MEAN SQUARE DEVIATION OF THE BOND ANGLE σ_θ COMPARED TO EXAFS EXPERIMENT.

structure	N_c	\bar{r}	σ_r	$\bar{\theta}$	σ_θ
A	3.87	2.36	0.08	108.63	14.25
B	3.84	2.36	0.07	108.64	11.94
C	3.84	2.35	0.07	108.52	13.80
D	3.89	2.37	0.08	108.35	15.85
E	3.82	2.38	0.07	108.67	13.69
average	3.85	2.36	0.07	108.56	13.91
exp. Ref. [24]	3.88	2.35	0.07	–	–

one overcoordinated and one undercoordinated atom each. Even though there is no one to one correspondence between a structural defect and a spectral defect state (as pointed out by Drabold et al. [26]), we were able to assign all spectral defects to defect atoms. As it can be seen in Fig. 7 the samples A and C have a clear gap without any defect states. The calculated density of states of the remaining samples is shown in Fig. 8.

TABLE V

TYPES OF NEIGHBORING ENVIRONMENTS FOR THREE STRUCTURES PREPARED BY FAST, NORMAL AND SLOW COOLING RATES. THE EXPRESSION Si_3H_1 DENOTES THAT THE GIVEN ATOM HAS A TOTAL NUMBER OF FOUR NEIGHBORS, THREE OF WHICH ARE SILICON ATOMS AND ONE IS A HYDROGEN ATOM.

structure	Si_2H_2	Si_3H_0	Si_3H_1	Si_4H_0	Si_4H_1	Si_5H_0
A	1	0	4	59	0	0
B	0	1	1	54	0	1
C	1	0	6	57	0	0
D	2	1	2	58	0	1
E	1	1	6	55	0	1

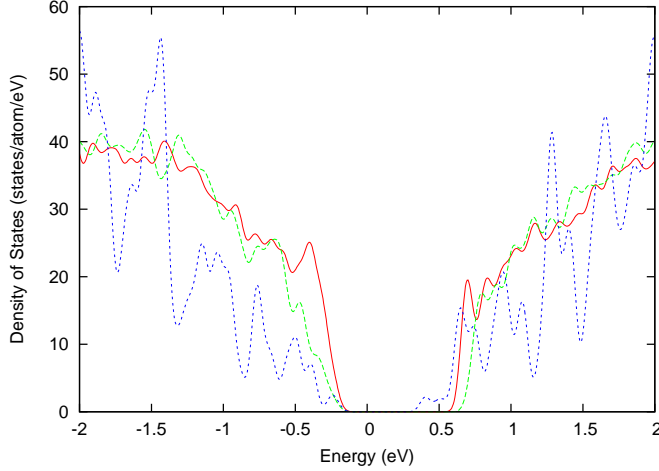


Fig. 7. Calculated density of states with a Gaussian smearing of 0.05 eV. Sample A (red solid line), sample C (green dashed line) and c-Si (blue dotted line). The Fermi Energy was set to 0 eV.

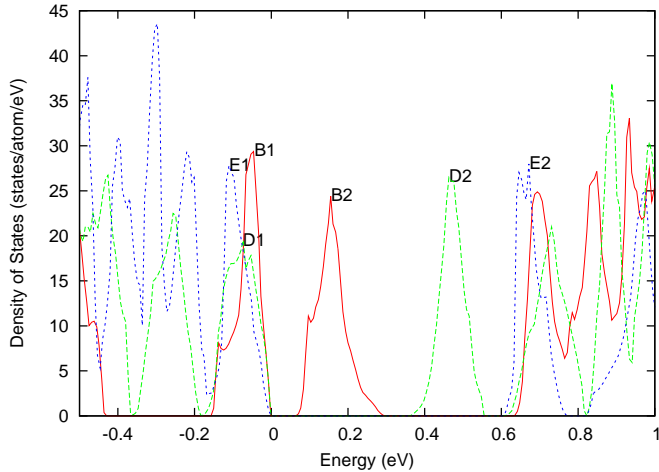


Fig. 8. Calculated density of states without smearing showing the ingap states of sample B (solid red line), sample D (dashed green line) and sample E (dashed blue line). The Fermi Energy was set to 0 eV, this is not necessarily the top of the valence band.

Each of the samples contains exactly two, strongly localized ingap states. We resolve these defect states as dangling bonds (three-fold coordinated atoms) and floating bonds (five-fold coordinated atoms). To be able to assign a particular ingap state to a corresponding defect atom, we project the charge

TABLE VI

SITE PROJECTED CHARGE DENSITY OF THE INGAP DEFECT STATES FOUND IN SAMPLES B, D AND E. THE LABEL “3 NEIGHBOR ATOMS” DENOTES THE SUM OF CHARGE DENSITY PROJECTIONS OVER THREE NEIGHBOR ATOMS OF AN UNDERCOORDINATED ATOM.

ingap state	undercoord. atom	3 neighbor atoms	overcoord. atom	5 neighbor atoms
B1	22.1	11.2	0.9	4.1
B2	2.5	4.1	7.7	35.2
D1	11.6	10.3	1.8	9.1
D2	1.6	2.8	9.7	33.2
E1	13.1	13.1	4.5	25.0
E2	25.2	8.7	2.5	32.4

TABLE VII

CALCULATED BAND GAP VALUES FOR THE FIVE SLOW QUENCH STRUCTURES.

sample	band gap [eV]
A	0.86
B	1.06
C	0.91
D	0.79
E	0.98
average	0.92

density of the ingap state onto spherical harmonics centered on each atom. The sum of the projections over all atoms is normalized to one. The site projected charge density of a total of six ingap states are summarized in Table VI. The defect state B1 situated under the Fermi energy is a dangling bond with 22 % of its charge density centered on an undercoordinated atom (see Fig. 9). Defect state B2 is a floating bond with the charge density localized on the neighbors of an overcoordinated atom (see Fig. 10). The situation is very similar in the D sample. Again we identify one dangling bond localized on an undercoordinated atom and one floating bond localized on the neighbors of an overcoordinated atom. Similarly the dangling bond state is under the Fermi level and the floating bond state is above. The interpretation becomes more difficult in the E sample. The state E2 (this time above the Fermi Energy) is a dangling bond with the charge density centered on the undercoordinated atom. However, for the E1 state it is difficult to decide whether it is a dangling or a floating bond. In this case the defect structures share their atoms and the charge density of the E1 state is contributing to both of them. The band gap values for all slow quench samples are summarized in Table VII. The average band gap is found to be 0.92 eV with a standard deviation of 0.10 eV. In general the DFT approximation underestimates band gaps. The calculated band gap of crystalline silicon is 0.6 eV, whereas the experimental value is 1.11 eV. Note that our calculated value of a-Si:H band gap is higher than the band gap of c-Si.

VIII. CONCLUSION

We performed an *ab initio* molecular dynamics simulation of a-Si:H. We examined the effect of the cooling rate on the quality of the amorphous structure and find a substantial improvement of structural and electronic properties with

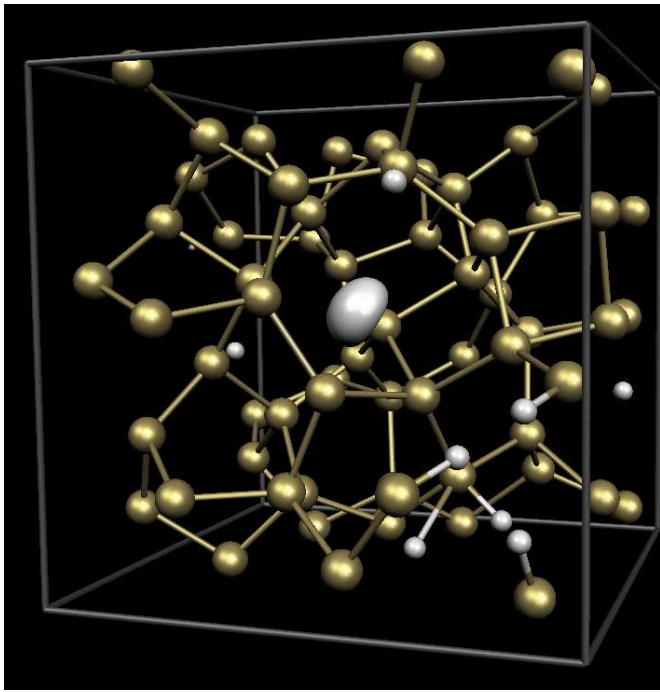


Fig. 9. Sample B containing 64 silicon (golden spheres) and 8 hydrogen (white spheres) atoms. The partial charge density of the defect state B1 is shown in gray color.

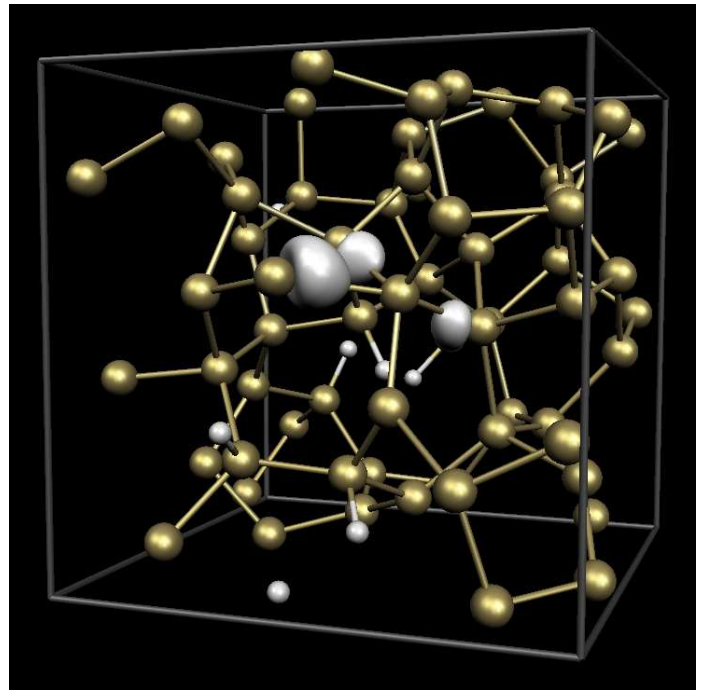


Fig. 10. Sample B containing 64 silicon (golden spheres) and 8 hydrogen (white spheres) atoms. The partial charge density of the defect state B2 is shown in gray color.

slower cooling. Further, we were able to reconstruct the experimental static structure factor and radial distribution functions obtained by neutron scattering measurements. Other structural properties like the coordination number N_c , mean nearest-neighbor distance \bar{r} , RMS deviation of the bond length σ_r , differ by no more than 1 % compared to values measured by EXAFS. Interestingly, the simulations reveal that the presence of hydrogen molecules in a-Si:H is possible. The slow quench samples contain a small number of defects. Two out of five slow quench samples contain neither structural defects nor spectral defect states in the gap. In the rest of the samples we find dangling and floating bond defects and couple them to undercoordinated and overcoordinated atoms respectively. The average band gap is found to be 0.92 eV with a deviation of 0.10 eV.

ACKNOWLEDGMENT

This work has been carried out with a subsidy of Dutch Ministry of Foreign Affairs under EOS-LT program and project number EOSLT02028.

This work is part of the research programme of the 'Stichting voor Fundamenteel Onderzoek der Materie (FOM)', which is financially supported by the 'Nederlandse Organisatie voor Wetenschappelijk Onderzoek (NWO)'.

REFERENCES

- [1] A. V. Shah, R. Platz, and H. Keppner, "Thin-film silicon solar cells: A review and selected trends," *Solar Energy Materials and Solar Cells*, vol. 38, no. 1–4, pp. 501–520, 1995.
- [2] F. Wooten, K. Winer, and D. Weaire, "Computer generation of structural models of amorphous si and ge," *Phys. Rev. Lett.*, vol. 54, p. 1392, 1985.

- [3] P. Keating, "Effect of invariance requirements on the elastic strain energy of crystals with application to the diamond structure," *Phys. Rev.*, vol. 145, no. 2, 1966.
- [4] F. Stillinger and T. Weber, "Computer simulation of local order in condensed phases of silicon," *Phys. Rev. B*, vol. 31, p. 8, 1985.
- [5] J. Tersoff, "Empirical interatomic potential for silicon with improved elastic properties," *Phys. Rev. B*, vol. 38, no. 14, 1988.
- [6] T. Ohira, T. Inamura, and T. Adachi, *Amorphous Silicon Technology 1994*, edited by E. A. Schiff, M. Hack, A. Madan, M. Powell, and A. Matsuda, *MRS Symposia Proceedings*, vol. 336, p. 177, 1994.
- [7] S. R. Billeter, A. Curioni, D. Fischer, and W. Andreoni, "Ab initio derived augmented tersoff potential for silicon oxynitride compounds and their interfaces with silicon," *Phys. Rev. B*, vol. 73, p. 155329, 2006.
- [8] D. Maroudas, "Modeling of radical-surface interactions in the plasma-enhanced chemical vapor deposition of silicon thin films," *Advances in Chemical Engineering*, vol. 28, p. 251, 2001.
- [9] S. Hara, S. Izumi, T. Kumagai, and S. Sakai, "Surface energy, stress and structure of well-relaxed amorphous silicon: A combination approach of ab initio and classical molecular dynamics," *Surface Science*, vol. 585, pp. 17–24, 2005.
- [10] R. Car and M. Parrinello, "Structural, dynamical, and electronic properties of amorphous silicon: An ab initio molecular-dynamics study," *Phys. Rev.*, vol. 60, no. 3, p. 204, 1988.
- [11] I. Stich, R. Car, and M. Parrinello, "Amorphous silicon studied by ab initio molecular dynamics: preparation, structure and properties," *Phys. Rev. B*, vol. 44, no. 20, p. 11092, 1991.
- [12] G. Servalli and L. Colombo, "Simulation of the amorphous-silicon properties and their dependence on sample preparation," *Europhys. Lett.*, vol. 22, no. 2, pp. 107–112, 1993.
- [13] I. Lee and K. Chang, "Atomic and electronic structure of amorphous si from first principles molecular-dynamics simulations," *Phys. Rev. B*, vol. 50, no. 24, pp. 18 083–18 089, 1994.
- [14] E. Kim and Y. Lee, "Structural, electronic, and vibrational properties of liquid and amorphous silicon: tight binding molecular dynamics approach," *Phys. Rev. B*, vol. 49, no. 3, p. 1743, 1994.
- [15] B. Tuttle and J. Adams, "Structure of a-si:h from harris-functional molecular dynamics," *Phys. Rev. B*, vol. 53, no. 24, pp. 16 265–16 271, 1996.

- [16] N. C. Cooper, C. M. Goringe, and D. R. McKenzie, "Density functional theory modelling of amorphous silicon," *Comput. Materials Science*, vol. 17, pp. 1–6, 2000.
- [17] V. Ivashchenko, P. Turchi, V. Shevchenko, L. Ivashchenko, and G. Rusakov, "Tight-binding-molecular-dynamics investigation of the atomic and electronic structure properties of a-c, a-si and a-sic," *Diamond and Related Materials*, vol. 12, pp. 993–997, 2003.
- [18] A. Valladares, F. Alvarez, Z. Liu, J. Sticht, and J. Harris, "Ab initio studies of the atomic and electronic structure of pure and hydrogenated a-si," *Eur. Phys. J. B*, vol. 22, pp. 443–453, 2001.
- [19] G. Barkema and N. Mousseau, "High-quality continuous random networks," *Phys. Rev. B*, vol. 62, no. 8, p. 4985, 2000.
- [20] G. Kresse and J. Hafner, "Ab initio molecular dynamics for liquid metals," *Phys. Rev. B*, vol. 47, no. 1, pp. 558–561, Jan 1993.
- [21] G. Kresse and J. Furthmüller, "Efficient iterative schemes for ab initio total-energy calculations using a plane-wave basis set," *Phys. Rev. B*, vol. 54, no. 16, pp. 11 169–11 186, Oct 1996.
- [22] P. E. Blöchl, "Projector augmented-wave method," *Phys. Rev. B*, vol. 50, no. 24, pp. 17 953–17 979, Dec 1994.
- [23] G. Kresse and D. Joubert, "From ultrasoft pseudopotentials to the projector augmented-wave method," *Phys. Rev. B*, vol. 59, no. 3, pp. 1758–1775, Jan 1999.
- [24] A. Filipponi, F. Evangelisti, M. Benfatto, S. Mobilio, and C. R. Natoli, "Structural investigation of a-si and a-si:h using x-ray-absorption spectroscopy at the si k edge," *Phys. Rev. B*, vol. 40, no. 14, pp. 9636–9643, Nov 1989.
- [25] R. Bellissent, A. Menelle, W. Howells, A. Wright, T. Brunier, R. Sinclair, and F. Jansen, "The structure of amorphous si:h using steady state and pulsed neutron sources," *Physica B*, vol. 156–157, pp. 217–219, 1989.
- [26] D. Drabold, P. Fedders, S. Klemm, and O. Sankey, "Finite temperature properties of amorphous silicon," *Phys. Rev. Lett. B*, vol. 67, no. 16, pp. 2179–2182, 1991.